2.L

Nuclear Physics **A140** (1970) 129—140; © *North-Holland Publishing Co., Amsterdam*

A STUDY OF DEUTERON SCATTERING ON ^{12}C AND ^{13}C

H. GURATZSCH, J. SLOTTA and G. STILLER

Zentralinstitut für Kernforschung, Bereich "Kernphysik", Rossendorf, DDR

Received 9 June 1969

Abstract: An optical-model analysis is presented of elastic deuteron scattering from ^{12}C and ^{13}C, measured at 13.7 MeV, and of other elastic deuteron scattering data from ^{12}C in the energy range 9–14 MeV. Good fits have been obtained with smooth energy dependence of the deduced parameters. DWBA calculations were carried out for inelastic scattering from ^{12}C.

E

NUCLEAR REACTIONS $^{12,13}C$(d, d), (d, d'), E = 13.7 MeV; measured $\sigma(\theta)$; deduced optical model parameters. Natural, enriched targets.

1. Introduction

In recent years, deuteron scattering on carbon isotopes has been investigated at intermediate energies [1–5]). Analyses of ^{12}C(d, d) data in the energy range 9–14 MeV with a simple potential, established the applicability of the optical model to light nuclei [2]). Satchler [3]) has shown that a reasonable optical-model description of the ^{12}C(d, d_0) differential cross sections can be obtained in the broad energy region 3–34 MeV. The ^{13}C(d, d_0) elastic scattering was investigated [5]) from 4 to 6 MeV. No experimental data, however, are available for inelastic scattering on ^{13}C.

In this work, differential cross sections of elastic and inelastic deuteron scattering on ^{12}C and ^{13}C were measured at E_d = 13.7 MeV. Optical-model analyses of the elastic-scattering data were carried out in conjunction with analyses of other ^{12}C(d, d) differential cross-section [2, 7–9]) and polarization [6]) data in the energy range 9–14 MeV. Attention has been paid to comparisons between ^{12}C and ^{13}C results and between cross-section [2, 9]) and polarization [6]) data available at E_d = 11.9 MeV.

The deduced optical parameters were used in some DWBA analyses of the inelastic-scattering data. The possibility of good theoretical descriptions with collective excitations for the ^{12}C nucleus has been established by Hinterberger *et al.* [10]). In the case of ^{13}C, a microscopic DWBA description based on a pure single-particle excitation was attempted.

2. Experimental method

The investigation of deuteron scattering at 13.7 MeV was performed with ^{13}C enriched targets in conjunction with natural carbon targets. The incident energy was

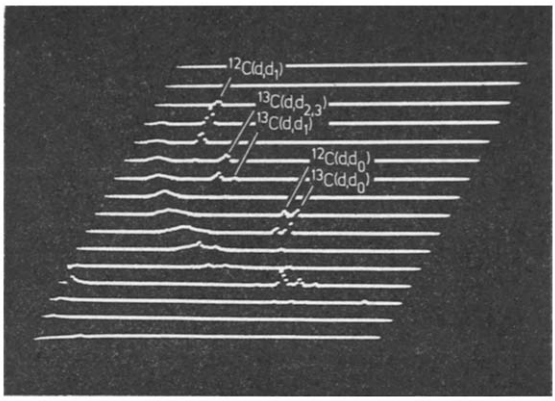

Fig. 1. Two-dimensional dE/dx versus E spectrum at $E_d = 13.7$ MeV and $\theta_{lab} = 150°$.

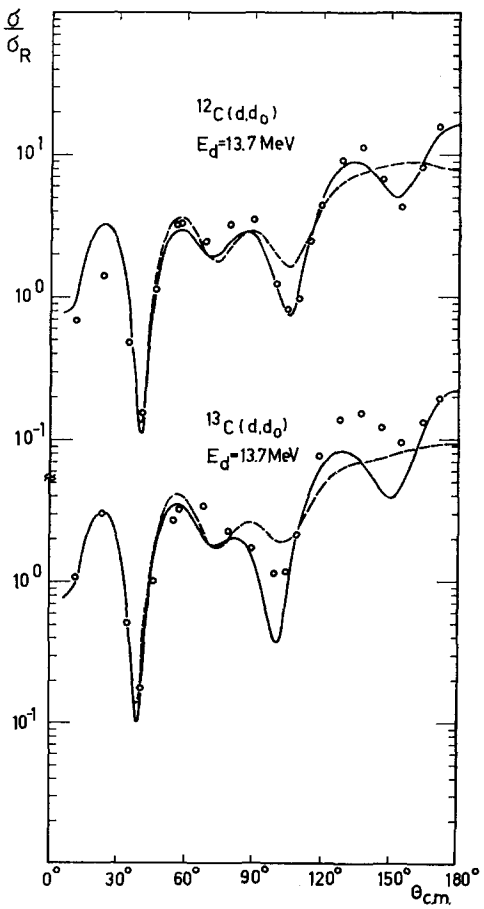

Fig. 2. Differential cross sections $^{12}C(d, d_0)$ and $^{13}C(d, d_0)$ at $E_d = 13.7$ MeV. Full curve – optical-model calculation with interpolated parameters (table 4) from set 1; dashed curve – calculated with parameters from set 2.

determined within an uncertainty of ± 0.1 MeV by comparing the energy of α-particles from the $^{12}C(d, \alpha)$ reaction with that from ThC-ThC′ α-particles. Natural and enriched carbon targets with a thickness of ≈ 0.6 mg/cm^2 were produced by

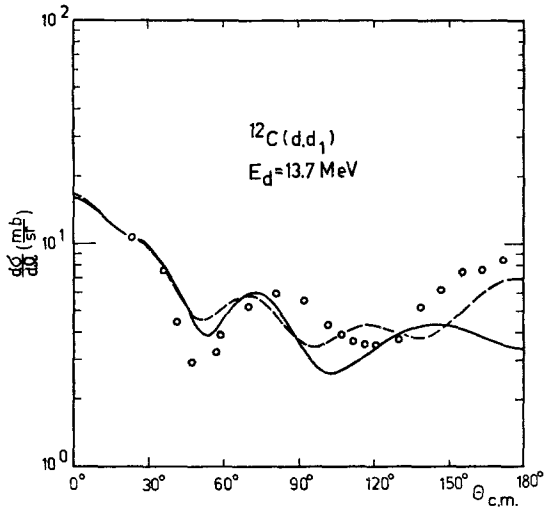

Fig. 3. Differential cross section $^{12}C(d, d_1)$ at $E_d = 13.7$ MeV compared with collective-model DWBA calculations. Full curve – DWBA calculation with optical parameters (table 4) from set 1; dashed curve – calculated with parameters from set 2.

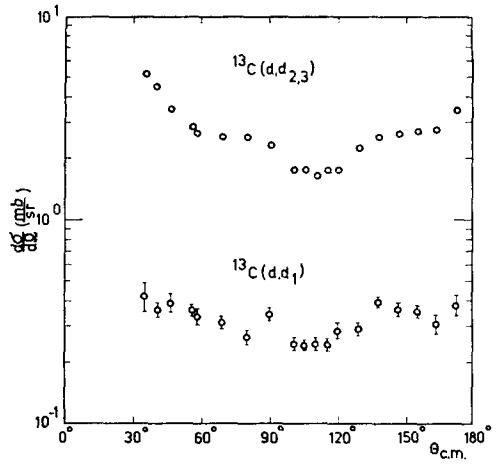

Fig. 4. Differential cross sections $^{13}C(d, d_1)$ and $^{13}C(d, d_{2+3})$ at $E_d = 13.7$ MeV.

cracking methyl iodide on a heated platinum disk. Absolute ^{12}C and ^{13}C contents in the enriched targets were determined by comparing the $^{12}C(d, p_0)$ and $^{13}C(d, p_0)$ stripping peaks at $\theta_{lab} = 58°$ from the enriched targets and from a polystyrene target.

(The natural abundance of ^{13}C is known [11]) to be 1.108 ± 0.004 %.) The ^{13}C enrichment thus obtained amounted to 54 ± 1 %.

Particles were detected with solid-state detectors (E and dE/dx method) in conjunction with a two-dimensional pulse-height analyser (fig. 1). In order to control the $^{12}C/^{13}C$ ratio of the targets during irradiation, spectra at $\theta_{lab} = 150°$ with separated $^{12}C(d,d_0)$ and $^{13}C(d, d_0)$ peaks were measured regularly. As the time of the measurement was short, no variation of the $^{12}C/^{13}C$ ratio was observed within the limits of accuracy of these checks.

3. Experimental results

The measured elastic differential cross sections $^{12}C(d, d_0)$ and $^{13}C(d, d_0)$ and the results of optical-model calculations are plotted in fig. 2. The angular distributions of the $^{12}C(d, d_0)$ and $^{13}C(d, d_0)$ cross sections show a similar diffraction pattern apart from the angular region $60° - 110°$ c.m., where the angular distribution from ^{12}C has an additional maximum. In fig. 3, the differential cross section $^{12}C(d, d_1)$ is

TABLE 1
Mean experimental errors

Reaction	Δr (%)	Δa (%)	$\Delta\sigma/\sigma$ (%)
$^{12}C(d, d_0)$	3	10	13
$^{13}C(d, d_0)$	5	14	19
$^{12}C(d, d_1)$	3	10	13
$^{13}C(d, d_1)$	10	14	24
$^{13}C(d, d_{2+3})$	3	14	17

The full relative error of the differential cross sections $\Delta\sigma/\sigma = \Delta r + \Delta a$ (%), where Δr is the error of the relative cross sections and Δa the error of the absolute values.

compared with DWBA calculations. The inelastic-scattering results obtained from ^{13}C are plotted in fig. 4. The energy resolution in the measurement was not high enough to separate the transitions to the second and third excited states of ^{13}C, therefore, the sum of $^{13}C(d, d_{2+3})$ cross sections are given. Mean experimental errors of the results are listed in table 1.

4. Analysis of the data

The optical-model analyses were performed with the search code OPA [12]) with a potential

$$V_{opt}(r) = V_C(r, R_C) - (U + iW) f(r, a, R) + 4a' iW' \frac{d}{dr} f(r, a', R') + U_S \left(\frac{\hbar}{m_\pi c}\right)^2 \frac{(\boldsymbol{l} \cdot \boldsymbol{\sigma})}{r} \frac{d}{dr} f(r, a, R),$$

where

$$f(r, a, R) = [1+\exp((r-R)/a)]^{-1}, \qquad R = r_0 A^{\frac{1}{3}}.$$

The programme may fit either the differential cross section or the polarization.

TABLE 2

Optimum parameters of set 1 (three-parameter fit)

Target	Measurement	E_d (MeV)	U (MeV)	$W = W'$ (MeV)	U_s (MeV)	χ^2 [a])	σ_R (mb)
^{12}C	$\frac{d\sigma}{d\Omega}$	13.9	101.6	6.07	4.18	5.1	1212
		13.7	103.8	5.94	4.23	11.6	1211
		13.2	103.2	5.25	4.24	4.5	1178
		12.8	105.6	4.93	4.64	4.8	1166
		12.4	104.6	5.00	4.85	3.7	1170
		11.9	107.7	4.24	6.49	4.2	1138
		11.8 [b])	108.7	5.01	7.15	5.1	1187
		11.8 [c])	110.4	4.43	7.26	3.8	1156
		11.4	107.6	5.12	6.90	2.9	1191
		11.0	113.7	4.75	7.02	5.3	1179
		11.0 [c])	110.5	3.16	6.44	6.9	1050
		10.6	113.2	4.93	10.30	3.0	1195
		10.0 [c])	116.0	4.13	6.76	5.3	1146
		9.0 [c])	118.9	4.03	8.14	7.1	1152
^{13}C	$\frac{d\sigma}{d\Omega}$	13.7	100.5	5.04	5.32	6.2	1215

The geometrical parameters fixed to constant values are $r_0 = 1.0$ fm, $r'_0 = 2.0$ fm, $r_c = 1.5$ fm, $a = 0.8$ fm, $a' = 0.6$ fm.

[a]) Obtained taking an average experimental error of 10 % in the optical-model analyses.
[b]) Ref. [8]). [c]) Ref. [7]).

TABLE 3

Optimum parameters characterized by a deep spin-orbit potential of ≈ 12 MeV (three-parameter fits)

Target	Measurement	E_d (MeV)	U (MeV)	$W = W'$ (MeV)	U_s (MeV)	χ^2 [a])	σ_R (mb)
^{12}C	$\frac{d\sigma}{d\Omega}$	13.2	105.2	5.34	13.0	8.6	1188
		12.8	107.2	4.34	14.4	6.8	1125
		11.9	110.0	4.46	12.4	5.1	1156
		11.8 [b])	110.3	4.54	12.7	3.0	1159
		11.0	111.7	4.80	12.4	5.5	1182
		11.0 [b])	115.9	3.47	12.3	6.7	1089
		10.6	113.2	4.93	10.3	3.0	1195
		9.0 [b])	118.7	4.08	11.5	7.7	1155
^{12}C	P	11.9 [c])	112.4	4.05	12.2	197	1127

The geometrical parameters are given in table 2.

[a]) Obtained taking an average experimental error of 10 % in the optical-model analyses except for the polarization measurement at $E_d = 11.9$ MeV. [b]) Ref. [7]). [c]) Ref. [6]).

Considering the results of preliminary fits of the differential cross sections, values of the geometrical parameters suitable for all energies have been determined. They are similar to those proposed by Satchler [3]). The choice of a mixture of volume and surface absorption with equal magnitudes of the potential depths W and W' was favoured by comparatively small χ^2-values.

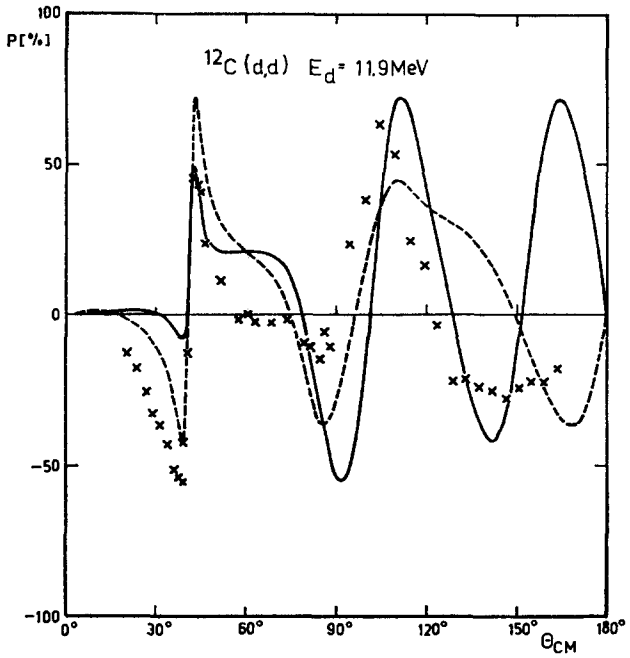

Fig. 5. Angular distribution of the polarization ^{12}C(d, d_0) at E_d = 11.9 MeV. Crosses – experimental results from ref. [6]), full curve – optical-model calculation with interpolated parameters (table 4) from set 1; dashed curve – calculated with parameters from set 2.

Fixing the geometrical parameters to the determined values (table 2), three-parameter fits of the differential cross sections were performed by varying the potentials U, $W = W'$ (as a group, equivalent to a single parameter) and U_s starting with initial values 100, 8 and 6 MeV, respectively. The results are listed in table 2. Except for the deuteron energy 10.6 MeV, spin-orbit potentials of $\approx$ 6 MeV have been obtained from these fits (set 1).

A spin-orbit potential $U_s \approx 12$ MeV, however, results (table 3) from analyses of the polarization at E_d = 11.9 MeV. Therefore, the differential cross sections were also fitted starting from this value of U_s = 12 MeV for the spin-orbit potential (table 3). At eight energies, second χ^2 minima with $U_s \approx 12$ MeV were found by the fitting procedure, but in some cases no minimum at $U_s \approx 12$ MeV exists. In order to study the influence of the spin-orbit potential, series of two-parameter fits on some typical data, viz. the polarization at 11.9 MeV and the differential cross sections at 11.9,

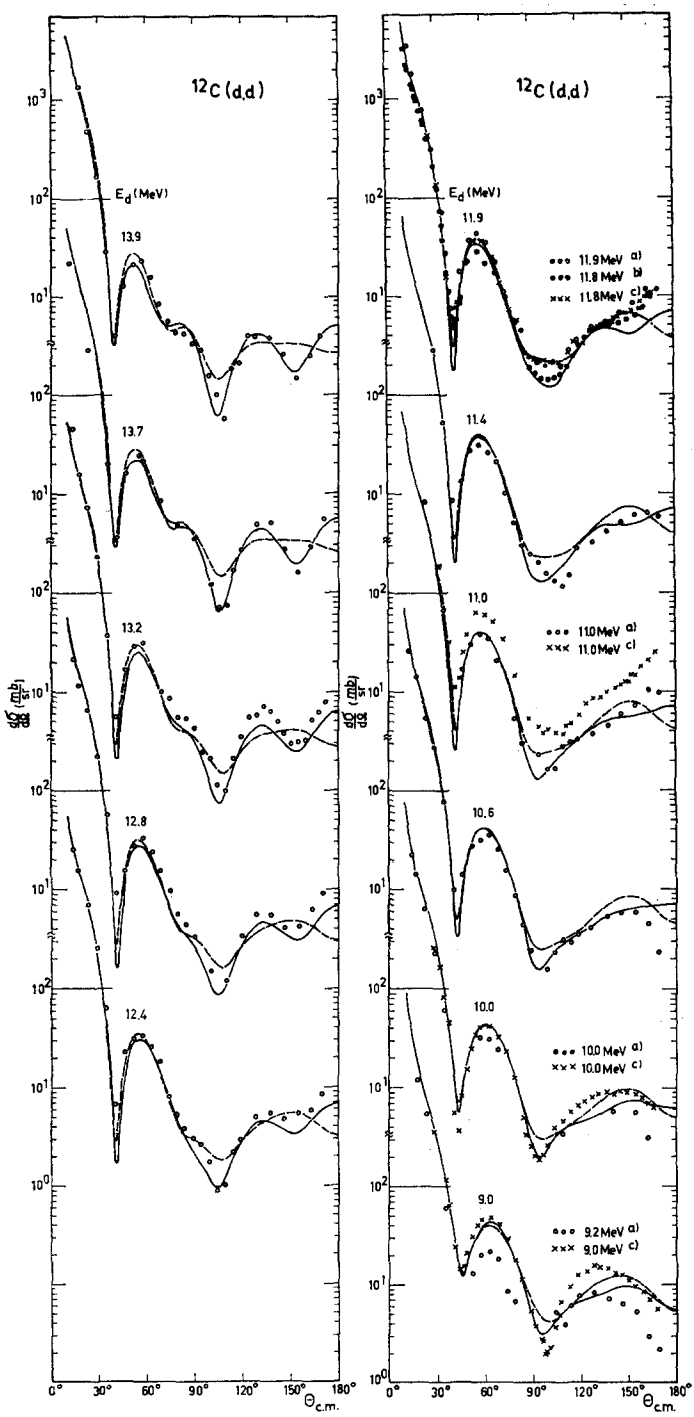

Fig. 6. Differential cross sections $^{12}C(d, d_0)$ in the energy range 9.0–13.9 MeV. Full curve – optical-model calculation with interpolated parameters (table 4) from set 1; dashed curve – calculated with parameters from set 2. a) Our measurements from refs. [2,9]). b) Data from ref. [8]). c) Data from ref. [7]).

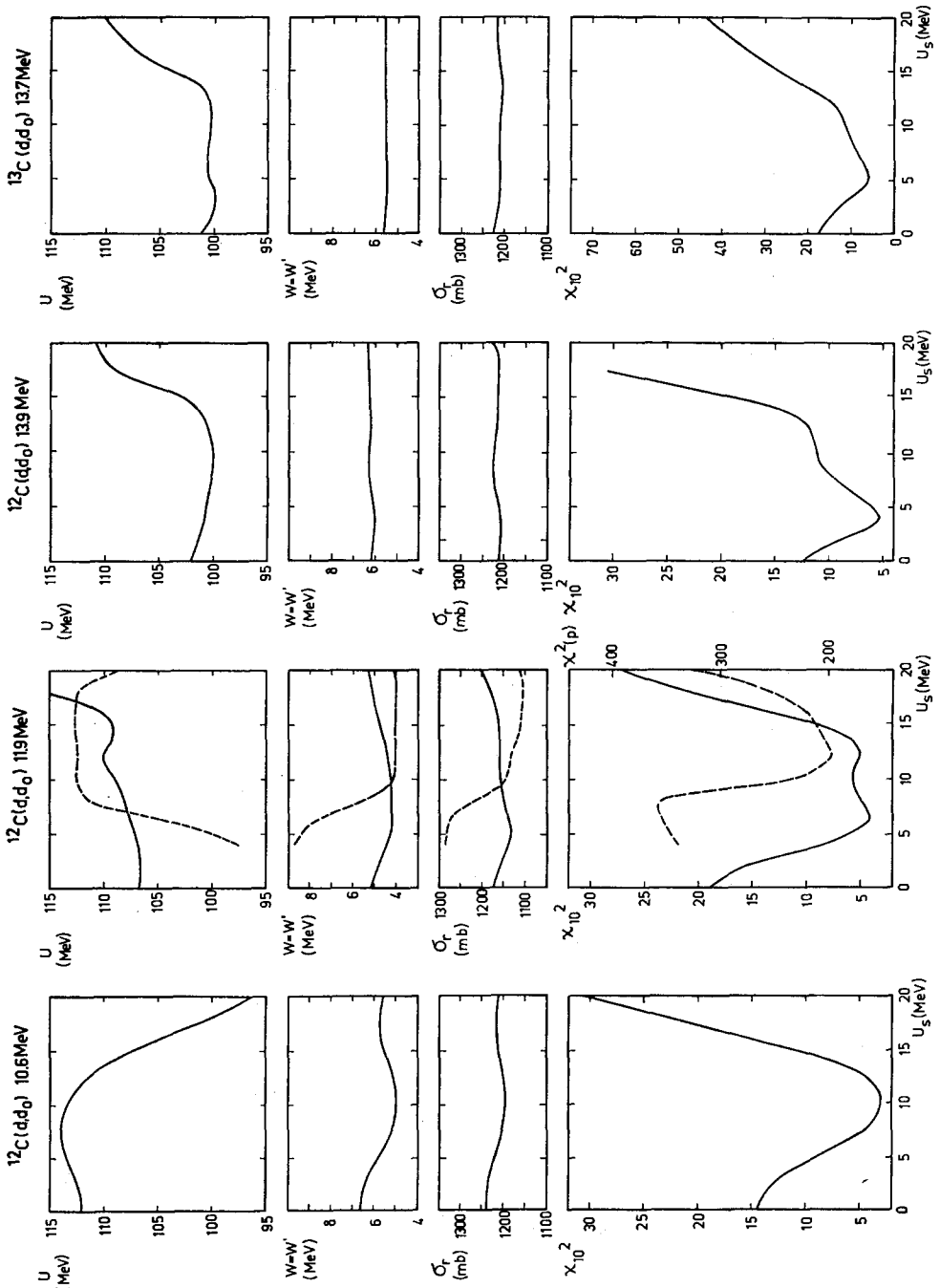

Fig. 7. Results of optical-model two-parameter fits (fitted U and $W = W'$) plotted versus the spin-orbit potential.

13.9 and 13.7 MeV were performed. The spin-orbit potential U_s was varied in 0.5 MeV steps from 0–20 MeV by the data input but was fixed during the fits. Fig. 7 shows plots of the fitted parameters U, $W = W'$, of the reaction cross section σ_r

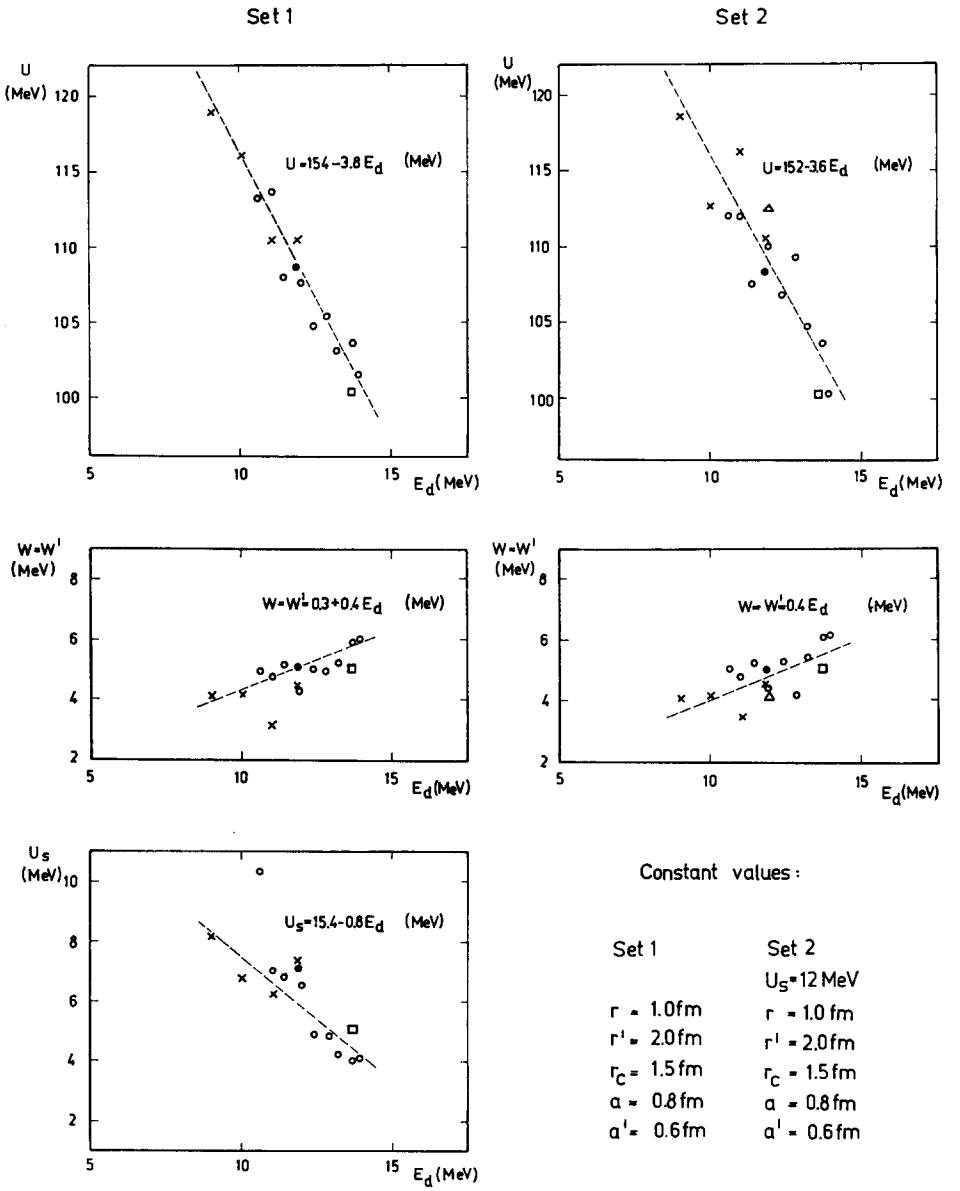

Fig. 8. Fitted optical parameters from tables 2 and 5 deduced from cross-section measurements: open dots – $^{12}C(d, d_0)$ own results [2,9]); dots – $^{12}C(d, d_0)$ ref. [8]); crosses – $^{12}C(d, d_0)$ ref. [7]); squares – $^{13}C(d, d_0)$ own results [9]), and polarization measurement: triangles – $^{12}C(d, d_0)$ ref. [6]), plotted versus energy.

and the χ^2 function versus the spin-orbit potential U_s. The χ^2 function from fitting the polarization has only one minimum at $U_s \approx 12$ MeV. Apart from the energy $E_d = 10.6$ MeV, a minimum at $U_s \approx 12$ MeV is found or indicated for the differential cross sections. The values of the other quantities U, $W = W'$ and σ_R derived from both the cross section and the polarization at $E_d = 11.9$ MeV are consistent at $U_s \approx 12$ MeV and differ strongly at $U_s \approx 6$ MeV.

TABLE 4

Optimum parameters of set 2 (two-parameter fits, $U_s = 12$ MeV)

Target	Measurement	E_d (MeV)	U (MeV)	$W = W'$ (MeV)	χ^2 [a]	σ_R (mb)
^{12}C	$\frac{d\sigma}{d\Omega}$	13.9	100.4	6.16	11.7	1220
		13.7	103.7	6.10	19.6	1219
		13.2	104.8	5.41	9.0	1195
		12.8	109.4	4.16	11.8	1126
		12.4	106.8	5.28	9.0	1196
		11.9	110.1	4.44	5.1	1156
		11.8 [b]	108.4	4.95	5.9	1186
		11.8 [c]	110.5	4.54	3.2	1163
		11.4	107.6	5.24	6.0	1202
		11.0	112.0	4.79	5.6	1183
		11.0 [c]	116.2	3.48	6.7	1092
		10.6	112.1	5.02	3.7	1196
		10.0 [c]	112.7	4.20	9.6	1157
		9.0 [c]	118.6	4.08	7.7	1154
^{12}C	P	11.9 [d]	112.5	4.09	197	1132
^{13}C	$\frac{d\sigma}{d\Omega}$	13.7	100.3	5.03	14.6	1206

The geometrical parameters are given in table 2.

[a]) Obtained taking an average experimental error of 10 % in the optical-model analyses except for the polarization measurement at $E_d = 11.9$ MeV.

[b]) Ref. [8]). [c]) Ref. [7]). [d]) Ref. [6]).

TABLE 5

Interpolation formulae for the optimum parameter sets 1 and 2

Parameter	Set 1	Set 2
U (MeV)	$154 - 3.8\,E_d$	$152 - 3.6\,E_d$
$W = W'$ (MeV)	$0.3 + 0.4\,E_d$	$0.4\,E_d$
U_s (MeV)	$15.4 - 0.8\,E_d$	12.0

The geometrical parameters fixed to constant values are $r_0 = 1.0$ fm, $r'_0 = 2.0$ fm, $r_c = 1.5$ fm, $a = 0.8$ fm, $a' = 0.6$ fm.

Since the deeper spin-orbit potential of ≈ 12 MeV is not only favoured by the analysis of the polarization but is also consistent with the analyses of the differential cross sections, two-parameter fits of all angular distributions were carried out by

varying U and $W = W'$. The spin-orbit parameter was fixed at 12 MeV, and thus provided for convergence also in such cases, where no separated χ^2 minimum exists (set 2). The results are listed in table 4. A survey on the fitted parameters of sets 1 and 2 (tables 2 and 4) plotted versus the incidence energy is given in fig. 8. The energy dependence of the parameters expressed by linear interpolation formulae (table 5) is smooth.

Parameters derived from these interpolation formulae were used to calculate the optical-model curves in figs. 2, 5 and 6.

At $E_d = 11.9$ MeV, the experimental differential cross section and polarization were changed within $\pm 20\,\%$ by varying the normalization factor. The dependence of the fitted parameters (three-parameter fits according to set 2) on these variations is small and of the same magnitude as indicated by the deviations of the single results from the interpolated values plotted in fig. 8.

TABLE 6

Real potential ambiguity for a deep spin-orbit potential in the elastic scattering $^{12}C(d, d_0)$ at $E_d = 11.9$ MeV (three-parameter fits)

Measurement	U (MeV)	$W = W'$ (MeV)	U_s (MeV)	χ^2 [a])	χ^2	σ_R (mb)
$\frac{d\sigma}{d\Omega}$	47.3	4.17	8.20	18.3		1077
P	42.3	7.41	10.3		263	1215
$\frac{d\sigma}{d\Omega}$	110.0	4.46	12.4	5.1		1156
P	112.4	4.05	12.2		197	1127
$\frac{d\sigma}{d\Omega}$	194.6	5.96	9.23	7.8		1279
P	198.8	10.6	14.2		299	1384

The geometrical parameters are given in table 2. The values of the differential cross sections are from refs. [2, 9]) and the polarizations from ref. [6]).

[a]) Obtained taking an average experimental error of 10 % in the optical-model analyses.

The real potential ambiguity for $U_s \approx 12$ MeV was investigated at 11.9 MeV by three-parameter fits (table 6). Smallest χ^2 values and best agreement between the parameters of the cross section and the polarization are found for a real potential of ≈ 100 MeV.

The inelastic scattering $^{12}C(d, d_1)$ was analysed by DWBA calculations (fig. 3) using the Rossendorf DWBA code [13]) with a collective-model form factor for doubly even nuclei [14]). The experimental angular distribution is reproduced with moderate success. From the normalization to the experimental data at forward angles, a value of $|\beta_2| = 0.5$ is obtained. It is consistent with the well-established result of $|\beta_2| = 0.6$ obtained by other investigations [10]).

The analysis of the inelastic scattering $^{13}C(d, d_1)$ by a microscopic DWBA description based on a pure single-particle excitation leads to an angular distribution

with pronounced diffraction pattern in disagreement with the measured results. The underestimation of experimental cross section suggests that core excitation might play a role.

5. Conclusions

The elastic deuteron scattering on ^{12}C and ^{13}C is well described by the optical model. The optimum parameters obtained show a smooth energy dependence that has been expressed by linear interpolation formulae. The results of set 1 are consistent with analyses carried out by Satchler [3]). The similarity of the parameters obtained from ^{12}C and ^{13}C completes the results published by Fitz *et al.* [15]), who found only small deviations between optical deuteron parameters deduced from measurements on ^{9}Be, ^{10}B, ^{11}B, ^{12}C, ^{14}N and ^{16}O at 11.8 MeV. Set 2 is favoured by the analyses of the polarization at 11.9 MeV and also gives a possible description for the differential cross section.

The deduced large value of $U_s \approx 12$ MeV is consistent with considerations [16]) that predict a deuteron spin-orbit potential equal to the sum of the proton and neutron spin-orbit potential.

We are indebted to Professor Dr. Schintlmeister for his steady interest in this work and to Dr. R. Reif for computational help in the microscopic analysis. H. Ulrich and M. Deutscher took care of solid-state detectors. The cyclotron staff provided an efficiently running machine.

References

1) P. E. Hodgson, Advan. Phys. **15** (1966) 329
2) F. Baldeweg *et al.*, Nucl. Phys. **84** (1966) 305
3) G. R. Satchler, Nucl. Phys. **85** (1966) 273
4) M. A. Melkanoff *et al.*, Phys. Lett. **2** (1962) 98
5) R. Cottrell *et al.*, Nucl. Phys. **A109** (1968) 288
6) A. M. Baxter *et al.*, Nucl. Phys. **A112** (1968) 209
7) G. G. Ohlsen and R. E. Shamu, Nucl. Phys. **45** (1963) 523
8) W. Fitz *et al.*, Nucl. Phys. **A101** (1967) 449
9) F. Baldeweg *et al.*, Report ZfK-168 (1969)
10) F. Hinterberger *et al.*, Nucl. Phys. **A115** (1968) 570
11) A. O. Nier, Phys. Rev. **77** (1950) 789
12) J. Slotta und G. Stiller, Report ZfK-142 (1968)
13) K. Hehl *et al.*, Report ZfK-151 (1968)
14) R. H. Bassel *et al.*, Phys. Rev. **128** (1962) 2693
15) W. Fitz *et al.*, Nucl. Phys. **A101** (1967) 449
16) J. Testoni and L. C. Gomes, Nucl. Phys. **89** (1966) 288